J Mater Sci: Mater Electron (2017) 28:8017–8022
DOI 10.1007/s10854-017-6506-5

Near-infrared quantum cutting and energy transfer mechanism in Lu_2O_3: Tm^{3+}/Yb^{3+} phosphor for high-efficiency photovoltaics

Wen Liu[1,2] · Jiahua Zhang[1] · Zhendong Hao[1] · Guotao Xiang[3] · LiangLiang Zhang[1] · Xia Zhang[1] · Guohui Pan[1] · Yongshi Luo[1] · Haifeng Zhao[1] · Huajun Wu[1]

Received: 2 November 2016 / Accepted: 30 January 2017 / Published online: 20 March 2017
© Springer Science+Business Media New York 2017

Abstract Near-infrared downconversion phenomenon has been demonstrated in Lu_2O_3: Tm^{3+}/Yb^{3+} phosphor upon direct excitation of Tm^{3+}:$^1G_4$ level at 463 nm. The efficient energy transfer from Tm^{3+}: $^1G_4 \rightarrow Yb$: $^2F_{5/2}$ has been elucidated by the excitation spectra, the visible and NIR spectra as well as the decay curves of Tm: $^1G_4$ state. The mechanism of downconversion in Lu_2O_3:Tm^{3+}/Yb^{3+} has been discussed in detail. According to analysis of the dependence of the initial transfer rate over Yb^{3+} ion concentration, it could be included that energy transfer (ET) from Tm^{3+} to Yb^{3+} is a single-step ET process instead of a cooperative one. By varying the Yb^{3+} concentrations, we obtain the Lu_2O_3: 0.2%Tm^{3+}/30%Yb^{3+} sample with theoretical quantum efficiency as high as 148.2%. Because the excited state of Yb^{3+} just above the band edge of crystalline silicon, it suggested that Lu_2O_3: Tm^{3+}/Yb^{3+} sample will be beneficial to improve the conversion efficiency of c-Si solar cells.

Keywords Downconversion · Energy transfer · Thulium–ytterbium system · Photovoltaics

✉ Jiahua Zhang
zhangjh@ciomp.ac.cn

[1] State Key Laboratory of Luminescence and Applications, Changchun Institute of Optics, Fine Mechanics and Physics, Chinese Academy of Sciences, 3888 Eastern South Lake Road, Changchun 130033, People's Republic of China

[2] Graduate School of Chinese Academy of Sciences, Beijing 100039, People's Republic of China

[3] Department of Mathematics and Physics, Chongqing University of Posts and Telecommunications, Chongqing 400065, People's Republic of China

1 Introduction

The long-run demand to exploit renewable, sustainable and clean energy sources continues to stimulate new approaches to manufacture of efficient and low-cost photovoltaic devices [1, 2]. At present, photovoltaic devices fabricated from silicon wafers dominating the marketplace possess a quite low efficiency of only 18% [3]. This is attributed to the large spectrum mismatch between solar radiation spectrum and the response spectrum of solar cells [4]. To circumvent this difficulty, either improvements in structure and composition of solar cells or modification of solar radiation spectrum has been suggested [5–8]. The spectral distribution of sunlight spectrum covers from 300 to 2500 nm at Air Mass 1.5 global (AM 1.5G), but only a small fraction around 800–1100 nm could be effectively utilized by silicon solar cells with 1.05 eV bandgap [9–11]. This is due to the higher reflection and absorption by the antireflection coatings optimized for longer wavelengths of solar cells [12]. To take advantage of high-energy photons with short wavelength, downconversion (DC) is considered as the most promising candidate for converting the incident high-energy photons into efficient near-infrared (NIR) photons to realize spectrum modification so far [13–15]. DC has been realized in RE^{3+}/Yb^{3+} couples, such as Er^{3+}/Yb^{3+}, Pr^{3+}/Yb^{3+}, Ce^{3+}/Yb^{3+}, Ho^{3+}/Yb^{3+} and Tm^{3+}/Yb^{3+} [16–20]. Yb^{3+} is suitable as an acceptor and emitter for the reason that the Yb^{3+} ion has an only excited state approximately 10,000 cm^{-1} just above the band edge of crystalline silicon [21]. Herein, we mainly focused on Tm^{3+}/Yb^{3+} couples which could convert blue photons around 463 nm into NIR photons around 1000 nm by efficient energy transfer from Tm^{3+} to Yb^{3+}. The wavelength at 1000 nm could be effectively utilized by solar cells.

The cubic rare earth sesquioxide Lu_2O_3 is selected as a host because of its chemically and environmentally stable properties [22]. On the contrary, the use of fluoride materials is restricted by their toxicity owing to the fluorine-containing species unlike the oxides [23]. It could also achieve a high rare-earth doping level in Lu_2O_3 [24]. Besides, Lu_2O_3 possesses a larger thermal conductivity (12.5 W/mk) [25] than YAG(10.7 W/mk) [26] making it more desirable for device manufacture. Recently, it has been reported that Lu_2O_3 is an excellent host for phosphors with efficient upconversion luminescence properties between Tm^{3+}/Yb^{3+}, Er^{3+}/Yb^{3+}, Ho^{3+}/Yb^{3+} couples [22, 27]. Moreover, strong downconversion luminescence in Tb^{3+} and Yb^{3+} codoped Lu_2O_3 has also been investigated [28]. However, little researches refer to downconversion between Tm^{3+}/Yb^{3+} combinations in Lu_2O_3 host and the transfer mechanism has not been demonstrated yet.

In this study, we report the efficient NIR DC in Lu_2O_3: Tm^{3+}/Yb^{3+} phosphor and analyze the energy transfer(ET) mechanism in Tm^{3+}/Yb^{3+} couples. We systematically demonstrate the DC process between Tm^{3+}/Yb^{3+} couples is a single-step ET process instead of a cooperative ET process assumed in other materials [29]. Visible and NIR emission spectra, decay time and energy transfer efficiency have been investigated in detail with varying Yb^{3+} concentration. Besides, the theoretical quantum efficiency as high as 148.2% has been obtained, well over the efficiency limit (29%) estimated by Shockley and Queisser [30]. Therefore, results show that Lu_2O_3 doped with Tm^{3+}/Yb^{3+} offers the opportunity for application in solar cells.

2 Experimental

2.1 Sample preparation

The series of samples investigated in this work with the general formula $Lu_{2-0.2\%-x\%}O_3$: 0.2%Tm^{3+}, x%Yb^{3+} (x = 0, 1, 5, 10, 20, 30) were prepared by a solid-state reaction. The oxides Lu_2O_3(4 N), Yb_2O_3(4 N), and Tm_2O_3(4 N) were employed as the raw materials, which were mixed homogeneously by an agate mortar for 30 min, placed in a crucible with a lid, then sintered at 1500 °C for 4 h.

2.2 Measurements and characterization

Powder X-ray diffraction (XRD) data was collected using Cu-Kα radiation (λ = 1.54056 Å) on a Bruker D8 advance diffractometer equipped with a linear position-sensitive detector (PSD-50m, M. Braun), operating at 40 kV and 40 mA with a step size of 0.01° (2θ) in the range of 10°–80°. The steady state excitation and emission spectra under direct excitation were measured using an FLS920 spectrometer (Edinburgh Instruments, U.K.). In energy level lifetime measurements, an OPO was used as an excitation source, and the signals were detected using a Tektronix digital oscilloscope (TDS 3052). The lifetimes were calculated by integrating the area under corresponding lifetime curves with the normalized initial intensity.

3 Results and discussion

The structures of Lu_2O_3 samples with nominal compositions 0.2% Tm^{3+}/ x% Yb^{3+} (x = 0, 1, 5, 10, 20, 30) were examined by typical powder X-ray diffraction pattern, as shown in Fig. 1. The positions and relative intensity of diffraction peaks for the powder samples can be well indexed to the standard cards of JPCD cards 12–0728. According to Fig. 1, there is no other phase in all XRD patterns. It demonstrates that Tm^{3+} and Yb^{3+} substitutions for Lu^{3+} sites have no effect on the phase structure.

In the UV region, high energy photons might be absorbed by either the Lu_2O_3 host or the rare-earth ions through charge transfer and f–d transitions. The possibility of the occurrence of DC is then clarified experimentally. To demonstrate the existence of DC from Tm: $^1G_4$ to Yb: $^2F_{5/2}$ in Lu_2O_3: Tm^{3+}/Yb^{3+} host, excitation spectra (PLE) was measured to be a direct evidence of DC as shown in Fig. 2. The intense excitation band centered at 463 nm is ascribed to $^1G_4 \rightarrow {}^3H_6$ transition when monitoring the Tm^{3+}: $^1G_4 \rightarrow {}^3F_4$, $^1G_4 \rightarrow {}^3H_5$, $^1G_4 \rightarrow {}^3H_4$ emission, respectively. Similarly, when monitoring the Yb^{3+}: $^2F_{5/2} \rightarrow {}^2F_{7/2}$ infrared emission at 980 nm, the excitation band could also be observed. This indicates the presence of direct ET from Tm^{3+} to Yb^{3+}. The weak excitation intensity for monitoring 980 nm emission of Yb^{3+} and 1200 nm emission of Tm^{3+}:

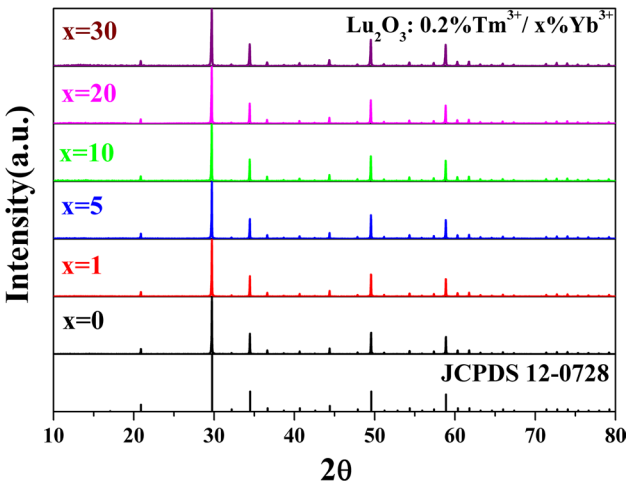

Fig. 1 The standard XRD data of Lu_2O_3 and the XRD patterns of the samples doped with different concentrations of Yb^{3+}

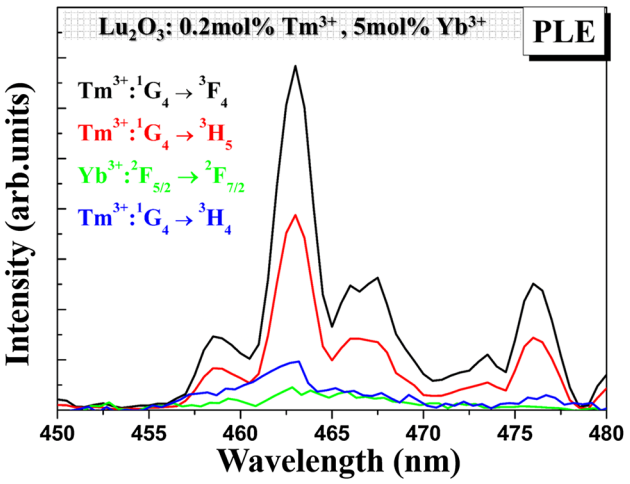

Fig. 2 Excitation spectra of $Tm^{3+:}\ {}^1G_4 \rightarrow {}^3F_4$, ${}^1G_4 \rightarrow {}^3H_5$, ${}^1G_4 \rightarrow {}^3H_4$ emission in Lu_2O_3: 0.2%Tm^{3+}/5%Yb^{3+} sample

${}^1G_4 \rightarrow {}^3H_4$ is because of lack of signal at infrared wavelength region for InGaAs detector used in present work.

As another direct evidence of $Tm^{3+} \rightarrow Yb^{3+}$ ET, the emission spectra covering from visible and NIR range of Lu_2O_3 samples with varying Yb^{3+} concentrations are depicted in Fig. 3. The emission peaked at 654 nm is originated from $Tm^{3+:}\ {}^1G_4 \rightarrow {}^3F_4$ transition. The group of emission lines at around 800 nm is corresponding to $Tm^{3+:}\ {}^1G_4 \rightarrow {}^3H_5$ transition. In the NIR region (900–1300 nm), the strong emission band peaked at 1024 nm is observed for the Tm^{3+} and Yb^{3+} codoped samples, which is responsible for $Yb^{3+:}\ {}^2F_{5/2} \rightarrow {}^2F_{7/2}$ transition under 463 nm Tm^{3+} excitation. The appearance of Yb^{3+} emission upon $Tm^{3+:}\ {}^1G_4$ excitation demonstrates the

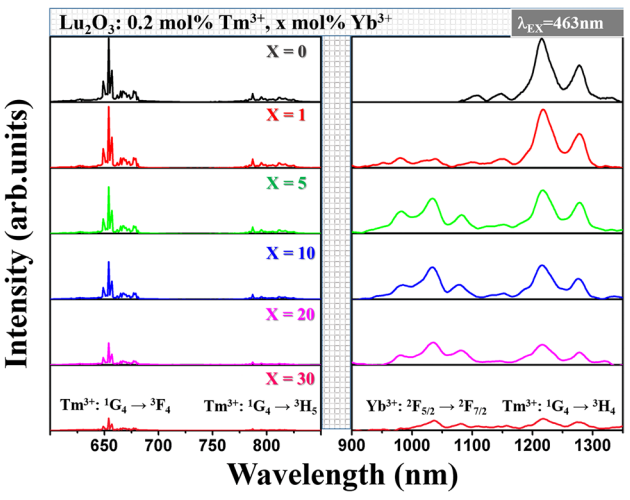

Fig. 3 Comparison of visible and NIR emission spectra of Lu_2O_3 samples with different Yb^{3+} doping levels and fixed 0.2%Tm^{3+} concentration under 463 nm excitation

effective energy transfer from Tm^{3+} to Yb^{3+}. The emission band in the range of 1100–1300 nm is assigned to $Tm^{3+:}\ {}^1G_4 \rightarrow {}^3H_4$ transition.

As depicted in Fig. 3, it can be concluded that the intensities of ${}^1G_4 \rightarrow {}^3F_4$, ${}^1G_4 \rightarrow {}^3H_5$, ${}^1G_4 \rightarrow {}^3H_4$ transition of Tm^{3+} have shown a markedly fast decrease with Yb^{3+} concentration increasing. Meanwhile, the NIR emission of Yb^{3+} increases rapidly when raising Yb^{3+} doping levels. This is attributed to the energy transfer process described as $Tm^{3+:}\ {}^1G_4 \rightarrow Yb^{3+:}\ {}^2F_{5/2}$ to convert blue photons into NIR photons. It is noticed that when the concentration of Yb^{3+} is over 5%, the intensity of Yb^{3+} emission decreases gradually, which is due to concentration quenching between Yb^{3+} ions. Therefore, 5 mol% denotes the optimal Yb^{3+} doped concentration in this series samples.

The PLE and PL spectra prove the energy transfer from Tm^{3+} to Yb^{3+} does exist in Lu_2O_3 host. For better understanding the energy transfer mechanism, the schematic thulium–ytterbium energy level diagram under 463 nm excitation with involved ET processes is depicted in Fig. 4. Upon 463 nm excitation, the Tm^{3+} ion in the ground state ${}^3H_4$ is populated to the upper ${}^1G_4$ level. The Tm^{3+} ions in the ${}^1G_4$ level may undergo two possible energy transfer routes: (1) Cooperative ET, as indicated in Fig. 4(a). As the excited energy level of Tm^{3+} donor ion is located at approximately twice the energy of that of Yb^{3+}, the DC mechanism was supposed to be a second-order cooperative ET process before [31]. A Tm^{3+} ion in the ${}^1G_4$ level transfers energy simultaneously to two nearby Yb^{3+} ions in the ground state and excites them to ${}^2F_{5/2}$ level, resulting in two emitting photons of Yb^{3+} with a wavelength around 1000 nm. (2)Single-step energy transfer, as shown in Fig. 4(b). A Tm^{3+} ion at ${}^1G_4$ state transfers energy to one Yb^{3+} nearby through a phonon-assisted ET process, leading to one NIR

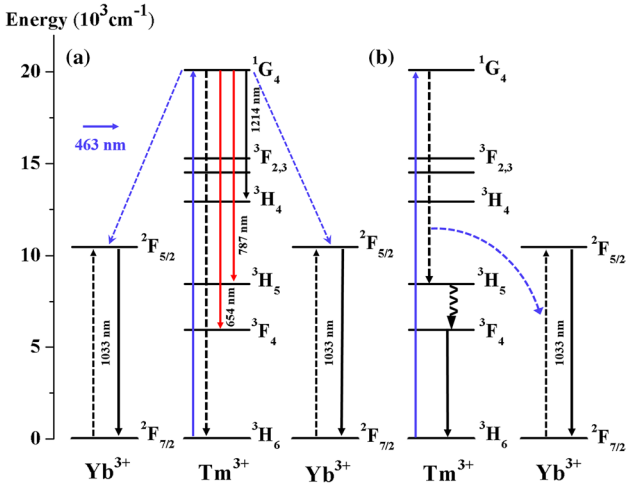

Fig. 4 Schematic thulium-ytterbium energy level diagram under 463 nm excitation including possible ET processes

emitting photon of Yb^{3+}. Meanwhile, it populates the $^3H_5$ state of Tm^{3+} and results in mid-NIR emission from $^3F_4$ state through fast nonradiative relaxation from $^3H_5$. It is known that cooperative ET is hard to occur because of the less probability of a second order ET comparing with a first-order one. In order to determine the real energy transfer process in Lu_2O_3: Tm^{3+}/Yb^{3+} system, the dependence of energy transfer rate upon Yb^{3+} ion concentration has been discussed. For the single-step energy transfer situation, the transfer rate of a Tm^{3+} ion at site 0 with a Yb^{3+} surrounding at site i can be described as.

$$W_{0i} = xf(R_{0i})X_0 \tag{1}$$

x denotes the concentration of the acceptor Yb^{3+} and thus could be representative of the probability of a Yb^{3+} at site i. X_0 is the radiative decay rate of $Tm^{3+:1}G_4$ state in Lu_2O_3. As a consequence, for all Tm^{3+} ions with Yb^{3+} neighboring at distances R_{0i}, the transfer rate for single-step energy transfer can be written as

$$W_{0S} = x\sum_i f(R_{0i})X_0 \tag{2}$$

It leads to

$$W_{0S} \propto \mathrm{x} \tag{3}$$

In this way, the energy transfer rate of single-step energy transfer is proportional to the acceptor concentration.

For the cooperative ET situation, one Tm^{3+} transfers its energy simultaneously to two Yb^{3+} adjacent at site i and j (i<j). According to Eq. (1), the transfer rate could be obtained as

$$W_0(i,j) = x^2 f(R_{oi})f(R_{oj}){X_0}^2 \tag{4}$$

Taking account into all the pairs of Yb^{3+} ions, the energy transfer rate of cooperative ET is

$$W_{0COOP} = x^2\sum_{i<j} f(R_{0i})f(R_{0j}){X_0}^2 \tag{5}$$

Thus, it could be deduced that

$$W_{0COOP} \propto x^2 \tag{6}$$

That is to say, the energy transfer rate of cooperative ET is proportional to the square of acceptor concentration.

The energy transfer rates are obtained from the decay curves of $Tm^{3+:}\ ^1G_4$ level in Lu_2O_3: $0.2\%Tm^{3+}$/ $x\%Yb^{3+}$ (x=0, 1, 5, 10, 20, 30) depicted in Fig. 5. A rapid decline in decay curves has been observed due to the existence of extra decay pathways with Yb^{3+} concentration increasing. Considerable energy transfer of $Tm^{3+:}\ ^1G_4 \rightarrow Yb^{3+:}\ ^2F_{5/2}$ accelerates the depopulation of $Tm^{3+:}\ ^1G_4$ state and leads to a variety of ET rates with different Yb^{3+} doping concentrations. All decay curves exhibit nonexponential characteristics. This result suggests that the radiative decay of Tm^{3+} might be accompanied by both multiphonon assisted relaxation and ET to adjacent

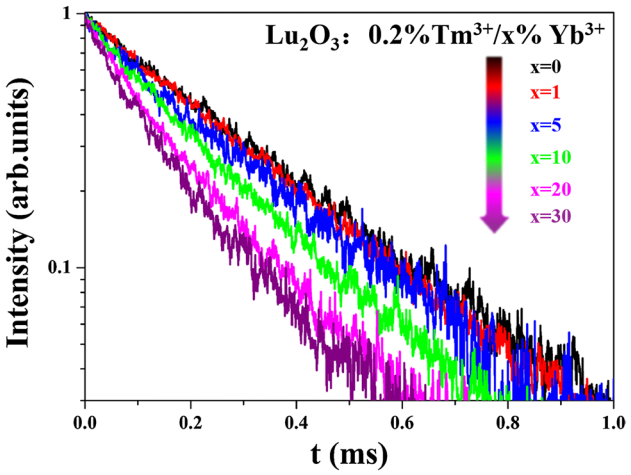

Fig. 5 Decay curves of $Tm^{3+:1}G_4$ state in Lu_2O_3: $0.2\%Tm^{3+}/x\%Yb^{3+}$ (x=0, 1, 5, 10, 20, 30) under 463 nm excitation

Yb^{3+} ions. We could calculate the lifetime by integrating the area under the corresponding decay curves with the normalized initial intensity at different Yb^{3+} doping levels. The lifetime results are presented in Table 1. The decay rate can be generally expressed by $W = W_r + W_{nr} + W_{ET}$, where W_r, W_{nr}, and W_{ET} are the radiative decay, non-radiative decay, and the ET rates. Accordingly, the energy transfer rate W_{ET} can be defined as

$$W_{ET} = \frac{1}{\tau} - \frac{1}{\tau_0} \tag{7}$$

where τ_0 and τ denote the average lifetimes of $Tm^{3+:}\ ^1G_4$ state in the absence and presence of energy transfer acceptors (Yb^{3+} ions). Consequently, we obtained the Yb^{3+} ion concentration dependence of the energy transfer rates and plotted in a double-logarithmic diagram, as shown in Fig. 6. When the concentration of Yb^{3+} ions changes from 1 to 30%, the slope is found to be around 1. It indicates that the Tm^{3+}-Yb^{3+} ET system is dominated by the single-step ET process rather than a cooperative ET process according to the analysis above. The possibility is quite low for $Tm^{3+} \rightarrow Yb^{3+}$ energy transfer to achieve DC with one-to-two photon emission in Lu_2O_3 material.

Based on the decay curves shown in Fig. 5, the energy transfer efficiency (η_{ETE}) and theoretical quantum efficiency (η_{TQE}) can be determined. The η_{ETE} is defined as the ratio of Tm^{3+} depopulated by energy transfer to Yb^{3+} over the total number of excited Tm^{3+} ions. Hence, the η_{ETE} could be expressed as a function of Yb^{3+} concentration by lifetimes

$$\eta_{ETE,x\%Yb} = 1 - \frac{\tau}{\tau_0} \tag{8}$$

where τ denotes the decay time of $Tm^{3+:}\ ^1G_4$ level with various concentrations of Yb^{3+}, the same as Eq. (7). For

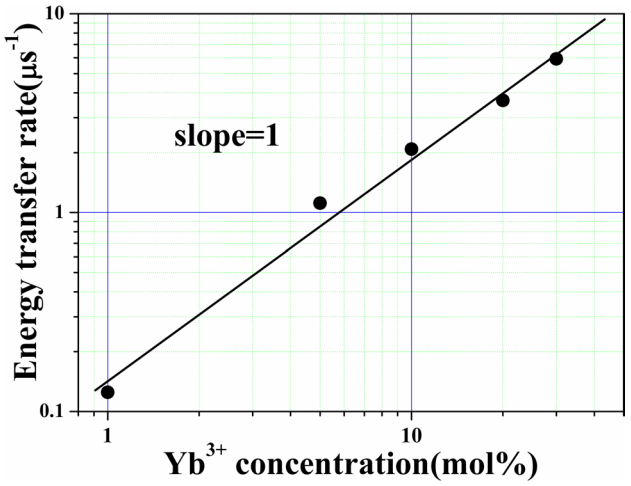

Fig. 6 Plot (log–log) of the energy transfer rate versus the Yb^{3+} concentration in Lu_2O_3: 0.2%Tm^{3+}/x%Yb^{3+} (x = 0, 1, 5, 10, 20, 30)

Table 1 Decay time, energy transfer efficiency (η_{ETE}) and theoretical quantum efficiency (η_{TQE}) as functions of Yb^{3+} concentration in Lu_2O_3: 0.2%Tm^{3+}/x%Yb^{3+} samples

x	Lifetime (μs)	η_{ETE} (%)	η_{TQE} (%)
0	260.2	0	100
1	250.1	3.9	103.9
5	233.3	10.3	110.3
10	189.6	27.1	127.1
20	152.7	41.3	141.3
30	134.7	48.2	148.2

the samples doped with x mol% Yb^{3+} ions (x = 1, 5, 10, 20, 30), the ET from Tm^{3+} to Yb^{3+} occurs by single-step ET process. In this way, one infrared photons is emitted by Yb^{3+} ions per absorbed one blue photon (around 463 nm) by Tm^{3+} ions in theory. Correspondingly, theoretical quantum efficiency (η_{TQE}) is defined as the ratio for the number of emitted photons over the number of absorbed photons. The relation between the energy transfer efficiency and the theoretical quantum efficiency is linear and can be expressed as

$$\eta_{TQE,x\%Yb} = \eta_{Tm}\left(1 - \eta_{ETE,x\%Yb}\right) + \eta_{Yb}\eta_{ETE,x\%Yb} + \eta_{Tm}\eta_{ETE,x\%Yb} \quad (9)$$

where η_{Tm} and η_{Yb} correspond to the quantum efficiencies of Tm^{3+} and Yb^{3+} ions, respectively. By assuming that all excited ions decay radiatively, their values are set to 1. This means nonradiative processes such as phonon-assisted relaxation, cross-relaxation between Tm^{3+} and Yb^{3+} as well as energy back transfer from Yb^{3+} to Tm^{3+} are all eliminated. The assumption can reach the upper limit of the theoretical quantum efficiency, the Eq. (9) thus can be simplified as

$$\eta_{TQE,x\%Yb} = 1 + \eta_{ETE,x\%Yb} \quad (10)$$

The η_{ETE} and η_{TQE} are listed in Table 1 based on the formulas mentioned above. The estimated η_{ETE} exhibits an obvious increase from 3.9 to 48.2% with increasing Yb^{3+} concentration. It is worth noticed that η_{TQE} reaches 148.2% for the Lu_2O_3: 0.2%Tm^{3+}/30% Yb^{3+} sample.

4 Conclusion

In this study, we demonstrate the efficient NIR downconversion in Tm^{3+} and Yb^{3+} codoped Lu_2O_3 samples. By measuring the excitation and emission spectra as well as the lifetime of $^1G_4$ level, effective energy transfer from $Tm^{3+:}$ $^1G_4$ to $Yb^{3+:}$ $^2F_{5/2}$ has been proved under 463 nm excitation. The dependence of the initial transfer rate upon Yb^{3+} concentration has been discussed to determine the downconversion process. It demonstrates that the ET from Tm^{3+} to Yb^{3+} occurs by single-step ET process. With raising Yb^{3+} doping level, a continuous increasing in theoretical quantum efficiency has been obtained by carefully calculation. The estimated maximum theoretical quantum efficiency reaches 148.2% in the Lu_2O_3: 0.2%Tm^{3+}/30%Yb^{3+} sample. As the main emission peak of Yb^{3+} in Lu_2O_3 around 1000 nm matches better with the optimal spectral response of the c-Si solar cell, it indicates that Lu_2O_3: Tm^{3+}/Yb^{3+} is promising DC material for application in solar cells.

Acknowledgements This work was partially supported by the National Key Research and Development Program of China (Grant No. 2016YFB0701003, 2016YFB0400605), National Natural Science Foundation of China (Grant No. 61275055, 11274007, 51402284 and 11604330), Natural Science Foundation of Jilin province (Grant No. 20140101169JC, 20150520022JH and 20160520171JH), and the prior sci-tech program of innovation and entrepreneurship of oversea Chinese talent of Jilin province.

References

1. S.E. Habas, HAS Platt, MFAM van Hest et al., Low-cost inorganic solar cells: from ink to printed device. Chem. Rev. **110**(11), 6571–6594 (2010)
2. K. Lee, J. Lee, B.A. Mazor et al., Transforming the cost of solar-to-electrical energy conversion: Integrating thin-film GaAs solar cells with non-tracking mini-concentrators. Light **4**(5), e288 (2015)
3. K. Yu, J. Chen, Enhancing solar cell efficiencies through 1-D nanostructures. Nanoscale Res. Lett. **4**(1), 1 (2008)
4. B.M. van der Ende, L. Aarts, A. Meijerink, Near-infrared quantum cutting for photovoltaics. Adv. Mater. **21**(30), 3073–3077 (2009)

5. J. Peet, J.Y. Kim, N.E. Coates et al., Efficiency enhancement in low-bandgap polymer solar cells by processing with alkane dithiols. Nat. Mater. **6**(7), 497–500 (2007)
6. M. Al-Ibrahim, O. Ambacher, S. Sensfuss et al., Effects of solvent and annealing on the improved performance of solar cells based on poly (3-hexylthiophene): fullerene. Appl. Phys. Lett. **86**(20), 201120 (2005)
7. X. Huang, S. Han, W. Huang et al., Enhancing solar cell efficiency: the search for luminescent materials as spectral converters. Chem. Soc. Rev. **42**(1), 173–201 (2013)
8. E.D. Kosten, J.H. Atwater, J. Parsons et al., Highly efficient GaAs solar cells by limiting light emission angle. Light. Sci. Appl. **2**(1), e45 (2013)
9. J.C. Arvesen, R.N. Griffin, B.D. Pearson, Determination of extraterrestrial solar spectral irradiance from a research aircraft. Appl. Optics **8**(11), 2215–2232 (1969)
10. B.S. Richards, Enhancing the performance of silicon solar cells via the application of passive luminescence conversion layers. Sol. Energy Mater. Sol. cells **90**(15), 2329–2337 (2006)
11. B.M. van der Ende, L. Aarts, A. Meijerink, Lanthanide ions as spectral converters for solar cells. Phys. Chem. Chem. Phys. **11**(47), 11081–11095 (2009)
12. C. Strümpel, M. McCann, G. Beaucarne et al., Modifying the solar spectrum to enhance silicon solar cell efficiency—an overview of available materials. Sol. Energy Mater. Sol. Cells **91**(4), 238–249 (2007)
13. Q.Y. Zhang, X.Y. Huang, Recent progress in quantum cutting phosphors. Prog. Mater. Sci. **55**(5), 353–427 (2010)
14. B.S. Richards, Luminescent layers for enhanced silicon solar cell performance: down-conversion. Sol. Energy Mater. Solar cells **90**(9), 1189–1207 (2006)
15. D.C. Yu, R. Martín-Rodríguez, Q.Y. Zhang et al., Multi-photon quantum cutting in Gd_2O_2S: Tm^{3+} to enhance the photo-response of solar cells. Light. Sci. Appl. **4**(10), e344 (2015)
16. L. Aarts, B.M. Van der Ende, A. Meijerink, Downconversion for solar cells in $NaYF_4$: Er, Yb. J. Appl. Phys. **106**(2), 023522 (2009)
17. G. Xiang, J. Zhang, Z. Hao et al., The energy transfer mechanism in Pr^{3+} and Yb^{3+} codoped β-$NaLuF_4$ nanocrystals. Phys. Chem. Chem. Phys. **16**(20), 9289–9293 (2014)
18. J. Li, L. Chen, Z. Hao et al., Efficient near-infrared downconversion and energy transfer mechanism of Ce^{3+}/Yb^{3+} codoped calcium scandate phosphor. Inorg. Chem. **54**(10), 4806–4810 (2015)
19. K. Deng, T. Gong, L. Hu et al., Efficient near-infrared quantum cutting in $NaYF_4$: Ho^{3+}, Yb^{3+} for solar photovoltaics. Opt. Express **19**(3), 1749–1754 (2011)
20. H. Lin, S. Zhou, X. Hou et al., Down-conversion from blue to near infrared in Tm–Yb codoped YO transparent ceramics. IEEE Photon. Technol. Lett. **22**(12), 866–868 (2010)
21. P. Vergeer, TJH Vlugt, MHF Kox et al., Quantum cutting by cooperative energy transfer in $Yb_xY_{1-x}PO_4$: Tb^{3+}. Phys. Rev. B **71**(1), 014119 (2005)
22. J. Yang, C. Zhang, C. Peng et al., Controllable red, green, blue (RGB) and bright white upconversion luminescence of Lu_2O_3: $Yb^{3+}/Er^{3+}/Tm^{3+}$ nanocrystals through single laser excitation at 980 nm. Chemistry **15**(18), 4649–4655 (2009)
23. A. Ulas, K.K. Kuo, C. Gotzmer, Ignition and combustion of boron particles in fluorine-containing environments. Combust. Flame **127**(1), 1935–1957 (2001)
24. R. Peters, C. Kränkel, K. Petermann et al., Crystal growth by the heat exchanger method, spectroscopic characterization and laser operation of high-purity Yb: Lu_2O_3. J. Cryst. Growth **310**(7), 1934–1938 (2008)
25. U. Griebner, V. Petrov, K. Petermann et al., Passively mode-locked Yb: Lu_2O_3 laser. Opt. Express **12**(14), 3125–3130 (2004)
26. A.I. Zagumennyi, G.B. Lutts, P.A. Popov et al., The thermal conductivity of YAG and YSAG laser crystals. Laser Phys. **3**(5), 1064–1065 (1993)
27. L. An, J. Zhang, M. Liu et al., Preparation and upconversion properties of Yb^{3+}, Ho^{3+}: Lu_2O_3 nanocrystalline powders. J. Am. Ceram. Soc. **88**(4), 1010–1012 (2005)
28. Li Li, Xiantao Wei, C. Yonghu et al., Energy transfer in Tb^{3+}, Yb^{3+} codoped Lu_2O_3 near-infrared downconversion nanophosphors. J. Rare Earths **30**(3), 197–201 (2012)
29. J. Li, J. Zhang, Z. Hao et al., Intense upconversion luminescence and origin study in Tm^{3+}/Yb^{3+} codoped calcium scandate. Appl. Phys. Lett. **101**(12), 121905 (2012)
30. W. Shockley, H.J. Queisser, Detailed balance limit of efficiency of p-n junction solar cells. J. Appl. Phys. **32**(3), 510–519 (1961)
31. J.M. Meijer, L. Aarts, B.M. van der Ende et al., Downconversion for solar cells in YF_3: Nd^{3+}, Yb^{3+}. Phys. Rev. B **81**(3), 035107 (2010)